ACS BIO & MED CHEM Au
AN OPEN ACCESS JOURNAL OF THE AMERICAN CHEMICAL SOCIETY

Editors' Choice
Open Access

pubs.acs.org/biomedchemau
Article

Mass Spectrometry-Based Protein Footprinting Defines the Binding Pocket of Crotonylated H3K14 in the PHD1 Domain of BAF45D within the BAF Chromatin Remodeling Complex

Marissa R. Martinez,[▽] Janna Kiselar,[▽] Benlian Wang, Dipti Sadalge, Laura Zawadzke, Asad Taherbhoy, Derek Musser, Yunji Davenport, Jeremy Setser, Mark R. Chance,* and Steve Bellon*

Cite This: *ACS Bio Med Chem Au* 2024, 4, 204–213

Read Online

ACCESS | Metrics & More | Article Recommendations | Supporting Information

ABSTRACT: The BRG-/BRM-associated factor (BAF) chromatin remodeling complex is a central actor in transcription. One mechanism by which BAF affects gene expression is via its various histone mark readers, including double plant homeodomains (DPF), located in the BAF45D subunit. DPF domains recognize lysine acetyl and acylations, including crotonylation, localized at promoters and enhancers. Despite a significant degree of conservation between DPF domains, attempts to crystallize BAF45D with a crotonylated histone 3 peptide (H3K14Cr) were unsuccessful. In addition, recent cryoEM and modeled structures failed to define the Req domain of BAF45D, which is responsible for reading lysine modifications. Thus, the precise mechanism of crotonyl group recognition and binding by BAF45D within the BAF complex remains unclear. We turned to protein footprinting mass spectrometry to map the binding interface between H3K14Cr and BAF45D. This technique is able to demarcate protein-binding interfaces by modifying surface-accessible residues and is not limited by protein size or composition. Experiments performed in the isolated DPF domain of BAF45D ($BAF45D_{DPF}$)-delineated H3K14Cr peptide binding across the PHD1 and PHD2 pockets. We observed markedly similar effects on the BAF45D subunit when assessing H3K14Cr binding in the purified full BAF complex. The ATPase motor, BRM, also displayed H3K14Cr-protected peptides in two separate domains that were subsequently evaluated in direct binding assays. These data confirm the BAF45D−crotonylamide interaction within its obligate complex and are the first to demonstrate H3K14Cr direct binding to BRM.

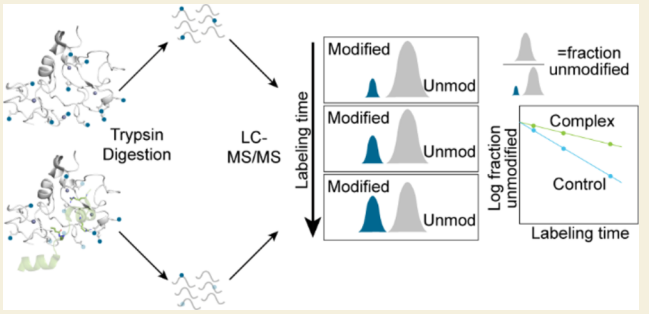

KEYWORDS: *protein footprinting, BAF, BRG-/BRM-associated factor, PHD, plant homeodomains, histone crotonylation, mass spectrometry*

INTRODUCTION

The post-translational modification of histone tails is essential to the initiation of gene transcription.[1−3] The discovery that lysine residues located at transcriptional start sites are modified by crotonylamide groups,[3] prompted focused research efforts into defining the structure−function relationship of this hydrophobic acylation as well as characterizing the enzymes and binding proteins that recognize and regulate it.

Key players in the recognition of histone tails are ATP-dependent chromatin remodeling complexes, such as BRG-/BRM-associated factor (BAF). BAF, a 1 MDa complex, is composed of 11 subunits that play specific roles in regulating gene transcription and are involved in tumor suppression.[4−7] The ability of BAF to recognize histone marks is derived from recognition domains spread across these various subunits. These include bromodomains (BRM/BRG; BRD7), chromodomains (BAF155/BAF170), double plant homeodomains (PHD;DPF) (BAF45D), and DNA binding domains, which work cooperatively to fine-tune gene regulation.[8−11]

The DPF domain of BAF45D (gene: DPF2) has been demonstrated to "read" various acetyl and acyl lysine modifications, including crotonylation.[12−15] BAF45D incorporates into the core BAF module through its Req domain, while its DPF domain is likely surface exposed, allowing it to perform its proposed reader functions.[16,17] DPF-containing proteins are also found in histone acetyl transferase complexes including the monocytic leukemic zinc finger protein (MOZ)/MOZ-related factor (MORF) (DPF subunit: MOZ),[18] where there is a

Received: February 16, 2024
Revised: May 14, 2024
Accepted: May 21, 2024
Published: June 17, 2024

significant degree of conservation between DPF domains.[14,15] These structures provide context for interpreting BAF DPF domains.

The PHD domain has a zinc finger architecture, composed of two antiparallel β sheets and a C-terminal α helix with a face-to-back orientation.[6,7,14] Within the first PHD (PHD1), a conserved Gly residue N-terminal to the His residue lines a binding pocket for Lys and its modifications. However, this Gly is substituted for a bulky aromatic residue in the second PHD domain (PHD2), obstructing the pocket and, presumably, preventing modified Lys from being recognized. MOZ binds various modified Lys residues but has the highest affinity for crotonylamide groups (5.8 μM). MOZ cocrystallized with a 25-mer crotonylated histone 3 tail peptide (H3K14Cr) (PDB 5B76) reveals the nature of this preference, whereby the planar crotonylamide group fits tightly inside the PHD1 pocket anchored by a hydrogen-bonding network. BAF45D has a similar preference for crotonylamide groups and binds with >50× stronger affinity (0.085 μM) compared with MOZ. However, attempts to crystallize BAF45D with H3K14Cr were unsuccessful, and thus, the precise mechanism of binding can only be inferred by comparison to models based on MOZ.

Covalent labeling of amino acids within proteins coupled with mass spectrometry, called protein footprinting, has been successfully applied to define antigen epitopes or binding interactions in binary and higher-order protein complexes.[19−22] Irreversible labeling techniques such as carboxyl group and hydroxyl radical footprinting modify surface-accessible side chains of amino acids, providing a readout of surface accessibility at the peptide and side-chain levels.[23−29] In the presence of a ligand or binding partner, the interaction surface can be excluded from access to the solvent, and the labeling of a given peptide or residue becomes attenuated. This technique is also capable of capturing allosteric changes, observed as decreased or enhanced labeling.[20,30,31] In contrast to other structural modalities, protein footprinting is amenable to proteins and interactions of various sizes and compositions and is sampled in solution, which extends characterization possibilities.

We employed protein footprinting to assess the mechanism of crotonyl peptide binding to BAF using both a purified BAF45D as well as a fully assembled and active BAF complex. We began our investigation with H3K14Cr binding to the BAF45D DPF domain ($BAF45D_{DPF}$). After showing similar binding affinity to previously published experiments, we used carboxyl group protein footprinting (Glu/E and Asp/D) to reliably map the binding interface between H3K14Cr and BAF45D as Glu and Asp residues were well distributed across all 11 subunits. We then expanded our system to the endogenous canonical BAF complex (1 MDa) purified using recently developed strategies.[4,17] In both systems, we observe protections along the PHD1 and PHD2 domains of BAF45D following H3K14Cr binding. Except for BRM, all other BAF subunits were unaffected. Direct binding assays were then performed for BRM to determine whether these alterations were due to direct binding or allosteric rearrangement. We combined these data with previously published structural models to gain insight into the nature of the H3K14Cr-BAF interaction. Our results confirm that the proposed mechanism of crotonyl peptide binding to canonical BAF is similar to BAF45D and reveal a potential novel histone reader target in BRM. Together, these data illustrate the power of protein footprinting methods to assess structure−function effects in large protein complexes and highlight new mechanisms of histone tail interactions by BAF.

MATERIALS AND METHODS

Materials

All materials were obtained from ThermoFisher Scientific (Waltham, MA) unless otherwise noted. Liquid chromatography−mass spectrometry (LC−MS) grade water and acetonitrile; 1× PBS, pH 7.8; and LysC and trypsin proteases. Glycine ethyl ester (GEE), 1-ethyl-3-(3-(dimethylamino)propyl) carbodiimide hydrochloride (EDC), Tris(2-carboxyethyl)phosphine hydrochloride (TCEP), ammonium acetate, and urea solution (8 M) were purchased from Sigma-Aldrich (St. Louis, MO). H3K14Cr peptide was purchased from Vivitide (Gardner, MA).

Protein Production

A construct containing the BAF45D PHD1 and PHD2 domains (237-391) was cloned in pET28a with an N-terminal 6x-Histidine tag, Avitag, and TEV cleavage site and expressed in *Escherichia coli* (N-His-TEV-Avitag-GSGS-BAF45D (237-391)). Protein was purified on a HisTrap HP column (Cytiva, Marlborough, MA) and eluted with 500 mM imidazole. Protein was digested by TEV protease (MilliporeSigma, Burlington, MA) and further purified by flow-through of HisTrap HP column. Protein was then loaded onto the Mono Q anion exchange column (Cytiva, Marlborough, MA), eluted with 300 mM NaCl, and further purified on a HiLoad 16/60 Superdex 75 (Cytiva, Marlborough, MA). Protein quality was checked by Coomassie-stained SDS-PAGE.

Fully assembled canonical BAF complexes were purified according to Mashtalir et al.[4] with slight modification. Briefly, CRISPR-Cas9 constructs for BRG1 knockout were transfected into HEK293T cells using Lipofectamine. Loss of BRG1 was confirmed by Western blot. BRG1 KO HEK293T cells were stably transfected with N106-BAF45D-FLAG. Cells were harvested and lysed, and FLAG-BAF45D-containing complexes were purified by anti-FLAG M2 affinity gel (MilliporeSigma, Burlington, MA). Complex integrity was confirmed by Coomassie-stained SDS-PAGE.

A construct containing the BRM bromodomain (1377-11486) was cloned in pET28a with an N-terminal 10xHis tag, PreScission Protease site, FLAG tag, and TEV protease site (pET28a-N-His10-3C-Flag-TEV-BRM (S1377-Q1486)). The protein was expressed in *E. coli*, purified by HisTrap Fast Flow column (Cytiva, Marlborough, MA), and eluted with 500 mM imidazole. Eluted protein was digested with His-tagged 3C PreScission protease (15 min, 20 °C), and protease was removed by flow-through of HisTrap HP column. Protein was loaded on the Mono Q anion exchange column and eluted with 300 mM NaCl. Protein was further purified on HiLoad 16/600 Superdex 75. Protein quality was checked by Coomassie-stained SDS-PAGE.

A construct containing the BRM ATPase domain (507−1326) was cloned in pFastbac1 with an N-terminal 6xHis tag, TEV protease site, and FLAG tag (pFastBac1-N-6xHis-FLAG-TEV-BRM(507−1326)). Protein was expressed in High Five cells and purified by anti-FLAG M2 affinity gel. Protein was further purified by HiLoad 16/600 Superdex 200 (Cytiva, Marlborough, MA). Protein quality was checked by Coomassie-stained SDS-PAGE.

AlphaLISA

AlphaLISA was used to assess H3K14Cr peptide binding to BAF45D and 3X FLAG-BAF. BAF45D or FLAG-BAF and increasing concentrations of H3K14Cr peptide were mixed and incubated together for 60 min in 20 mM HEPES (pH 7.5), 100 mM NaCl, 0.5 mM DTT, 0.005% Tween-20, and 0.005% BSA in a 384-well proxiplate. Following incubation, streptavidin donor beads (PerkinElmer, Waltham, MA) and anti-Flag M2 acceptor beads (PerkinElmer) were added to a final concentration of 20ug/mL and incubated for 60 min. Plates were read at an excitation of 680 nm and an emission at 615 nm on a PHERAstar plate reader (BMG Labtech, Ortenberg, Germany).

Protein Footprinting Mass Spectrometry and Analysis

All protein samples were purified into a buffer of 1× PBS, pH 7.8. The BAF-H3K14Cr or $BAF45D_{DPF}$-H3K14Cr peptide complexes were each formed at a 1:5 ratio. The protein concentrations of BAF and

https://doi.org/10.1021/acsbiomedchemau.4c00009
ACS Bio Med Chem Au 2024, 4, 204−213

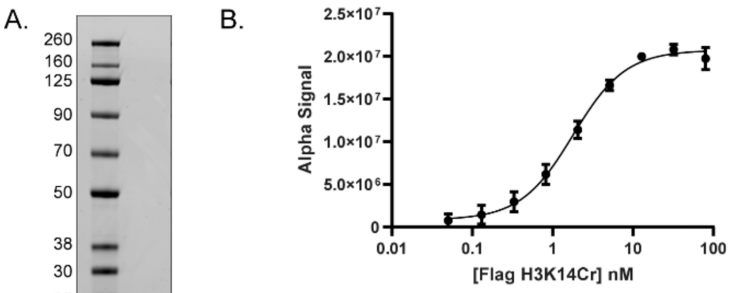

C.

Location	Sequence BAF45D	Protection Ratio
242-253	EDSQPPTPVSQR	1.01
261-281	KGPDGLALPNNYCDFCLGDSK	1.19
286-300	**TGQPEELVSCSDCGR**	**1.40**
301-318	SGHPSCLQFTPVMMAAVK	NL
322-328	**WQCIECK**	**3.41**
329-350	**CCNICGTSENDDQLLFCDDCDR**	**4.34**
351-379	GYHMYCLTPSMSEPPEGSW SCHLCLDLLK	1.05

Figure 1. DPF domain of BAF45D binds to H3K14Cr. (A) Construct containing the BAF45D PHD1 and PHD2 domains (237-391) was expressed in *E. coli* and purified to homogeneity as visualized by Coomassie-stained SDS-PAGE. (B) Biotinylated-BAF45D was incubated with increasing concentrations of Flag-tagged H3K14Cr peptide followed by the addition of streptavidin donor and anti-Flag acceptor beads (AlphaLISA). H3K14Cr bound BAF45D with an EC50 of 2.41 ± 0.5 nM, n = 3. (C) BAF45D was exposed to GEE/EDC labeling ± H3K14Cr peptide over a time course followed by LC−MS/MS and manual validation of peptide spectra. Modification rate constants (*K*fp) were calculated for each peptide, where PR= *K*fpBAF45D/*K*fpBAF45D-H3K14Cr. Peptides with a ratio >1.30 are considered protected (bold). Underlined residues indicate the conserved histone binding sequence within the PHD1 (298-306) and PHD2 (348-356) domains. NL= no labeling.

$BAF45D_{DPF}$ were adjusted to 0.5 and 10 μM with H3K14Cr peptides at 2.5 and 50 μM, respectively.

Protein samples were mixed with EDC (240 mM) and GEE (8 mM) in PBS for 0, 2.5, 5, and 6.5 min at room temperature and quenched with 8 M urea and 200 mM DTT in 1 M ammonium acetate. Excess labeling reagents were removed[32] followed by 10% TCA/acetone precipitation overnight at −20 °C with 3 washes of acetone. Samples were then resuspended in 50 mM Tris buffer, pH 8.5, reduced with 10 mM DTT at 56 °C for 45 min and alkylated with 25 mM iodoacetamide at room temperature in the dark for 45 min. Digestion was done with LysC for 3 h, followed by trypsin overnight at 37 °C using an enzyme-to-protein ratio of 1:10 (w/w).

Identification and quantification of modification sites were performed by LC−MS/MS using an Orbitrap Eclipse mass spectrometer (ThermoFisher Scientific, Waltham, MA) interfaced with a Waters nanoAcquity UPLC system (Waters, Milford, MA). The 500 ng and 200 ng of proteolytic peptides derived from BAF and $BAF45D_{DPF}$, respectively, were loaded on a trap column (180 μm × 20 mm packed with C18 Symmetry, 5 μm, 100 Å; Waters, MA) to desalt and concentrate peptides. These peptide mixtures were eluted on a reverse-phase column (75 μm x 250 mm column packed with C18 BEH130, 1.7 μm, 130 Å; Waters, MA) using a linear gradient of 2 to 42% mobile phase B (100% acetonitrile/0.1% formic acid) vs mobile phase A (100% water/0.1% formic acid) for 210 and 100 min, respectively, at 40 °C and a flow rate of 300 nL/min. Peptides were introduced into the nanoelectrospray source at a capillary voltage of 2.1 kV. MS1 spectra were acquired in the Orbitrap (R = 120 K: AGC target = 400,000; MaxIT = 50 ms; mass range = 350−1500). MS2 spectra were collected in the linear ion trap (AGC target 10,000; MaxIT = 35 ms; NCECID = 35%). The resulting MS/MS data were searched against canonical BAF subunits and BAF45D FASTA sequences using MassMatrix software to identify modification sites. MS/MS spectra were searched for tryptic peptides with mass accuracy of 10 ppm and 0.8 Da for MS1 and MS2 scans, respectively. Variable modifications included cysteine carbamidomethylation, methionine oxidation, and aspartate/glutamate modified by GEE (+85.0527 Da). MS/MS spectra for each site of the proposed modification were manually examined and verified.

ProtMap software was used to screen the data set for candidate peptides/regions likely to bind, which were subsequently manually validated. The extent of modification (fraction unmodified) for peptides and residues was quantified as a function of GEE/EDC labeling time using the integrated peak areas of the unmodified peptide (A_u), and of a peptide in which a residue is modified (A_m) derived from selected ion chromatograms as described previously.[20,21,33] Briefly, the fraction unmodified (F_u) for each specific modified species was calculated according to the following formula: $F_u = 1 - (A_m/(A_u + \sum A_m))$, where $\sum A_m$ is the sum of all modified products for a particular peptide. Dose−response curves were generated using unmodified fractions for each peptide (or specific site of modification) plotted versus labeling time. The dose−response curves were fit to an exponential decay function to generate the modification rate constants *K*fp for the labeling reaction over time (Figures S1 and S2). The protection ratios (PR) were calculated as the fraction of Kfp_{free} over $Kfp_{complex}$, where free refers to $BAF45_{DPF}$, BAF45D, or SMARCA2, and complex refers to the addition of H3K14Cr. For the histogram distribution of peptide data (Figure 2C), the ratios for all Flag-BAF peptides were calculated as a fraction of a specific modified peptide in the free Flag-BAF ($F_{ModFree}$) over the fraction of modified peptide in the Flag-$BAF_{H3K14Cr}$ ($F_{ModComplex}$). PR values <1 suggest that the corresponding region gained solvent accessibility due to structural changes in the complex, e.g., local unfolding (allostery), whereas PR > 1 reveals protection from solvent following complex formation driven by direct interaction or allostery. PR ∼ 1 indicates no change. As H3K14Cr is small (25 residues) relative to the size of BAF (∼10,000 residues), we expect most regions to show PR values close to 1 and be unaffected by binding.

RESULTS

$BAF45_{DPF}$ Recognition of H3K14Cr Revealed by GEE-Based Protein Footprinting

Recently, the recognition of varied lysine acyl groups on 25-mer histone tail peptides (H3K14) by isolated DPF domains of MOZ (MOZ_{DPF}) and BAF45D ($BAF45D_{DPF}$)[14] demonstrated a

https://doi.org/10.1021/acsbiomedchemau.4c00009
ACS Bio Med Chem Au 2024, 4, 204−213

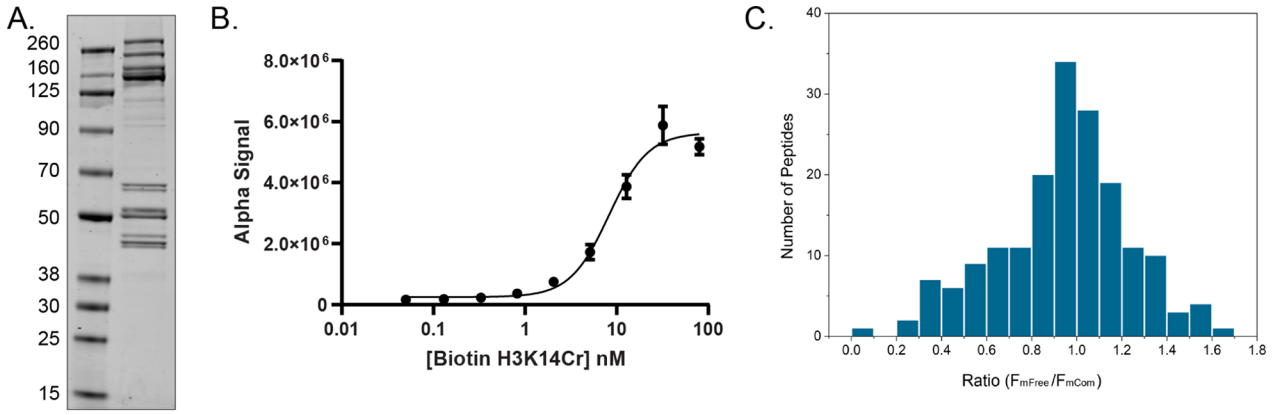

D.

Location	Sequence BAF45D within BAF	Protection Ratio
93-107	LSFPSIKPDTDQTLLK	0.44
109-124	EGLISQDGSSLEALLR	0.82
138-152	VDDDSLGEFPVTNSR	0.92
156-178	RILEPDDFLDDLDDEDYEEDTPK	0.98
197-205	LDASILEDR	1.13
206-216	DKPYACDICGK	1.05
220-241	NRPGLSYHYAHSHLAEEEGEDK	0.64
242-253	EDSQPPTPVSQR	0.99
261-281	KGPDGLALPNNYCDFCLGDSK	1.23
286-300	**TGQPEELVSCSDCGR**	**1.33**
301-318	SGHPSCLQFTPVMMAAVK	NL
322-328	**WQCIECK**	**1.24**
329-350	**CCNICGTSENDDQLLFCDDCDR**	**1.50**
351-379	GYHMYCLTPSMSEPPEGSWSCH LCLDLLK	0.89
410-423	DHDGDYKDHDIDYK	0.57

E.

Location	Residue level Modification	Protection Ratio	
		BAF45D within BAF	BAF45D
261-281	D264	1.02	0.86
	D274	ND	2.37
	D279	1.07	0.93
286-300	E290	0.87	ND
	E291	1.15	1.12
	D297	1.29	1.40
322-328	E326	1.24	3.41
329-350	E337/D340	ND	1.28
	D339	ND	1.34
	D346	1.76	5.22
	D347	0.90	1.19
	D349	1.41	6.51

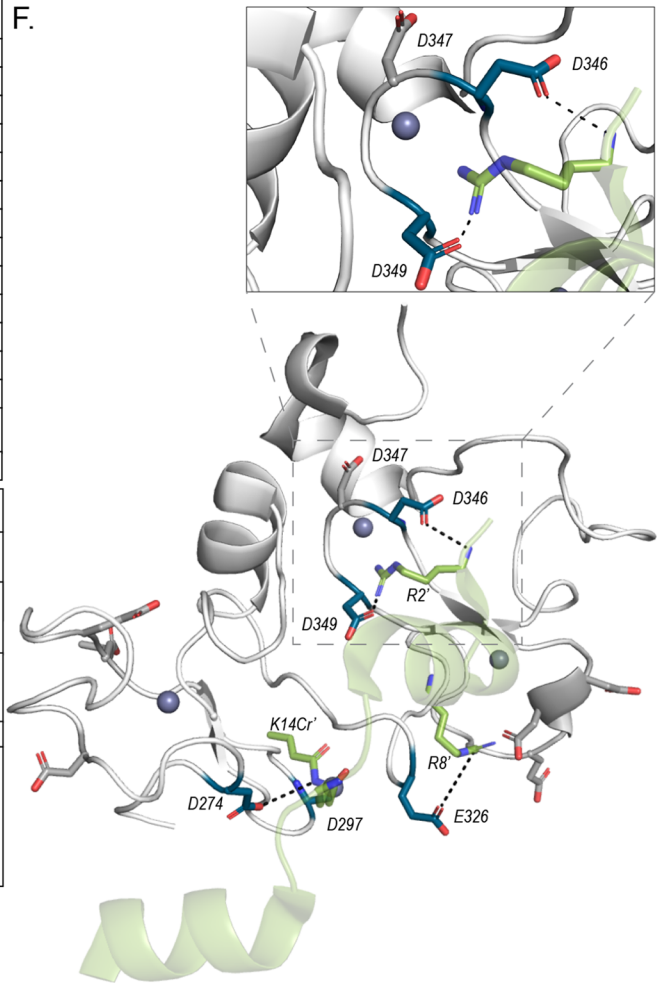

Figure 2. H3K14Cr is recognized by the DPF domain of BAF45D within the BAF complex. (A) BRG1 KO HEK293T cells were stably transfected with N106-BAF45D-FLAG. FLAG-tagged-BAF45D containing complexes (Flag-BAF) were purified by anti-FLAG M2 affinity gel. Complex integrity was confirmed by Coomassie-stained SDS-PAGE. (B) Flag-BAF was incubated with increasing concentration of biotinylated H3K14Cr peptide followed by the addition of streptavidin donor and anti-Flag acceptor beads (AlphaLISA). H3K14Cr bound Flag-BAF with an EC50 of 8.61 ± 0.5 nM, $n = 3$. (C) Flag-BAF was exposed to GEE/EDC labeling in the presence and absence of H3K14Cr peptide over a time course followed by LC−MS/MS and manual validation of peptide spectra. The distribution of ratios for all Flag-BAF peptides was binned and plotted in a histogram for the free Flag-BAF against the Flag-BAF-H3K14Cr. (D) Table of the PR for BAF45D peptides. Peptides with PR > 1.3 are significantly protected, while 322−328 is trending (bold). Underlined residues indicate the conserved histone binding sequence within the PHD1 (298−306) and PHD2 (348−356) domains. (E) Table of the PR for each Asp and Glu residue located within protected peptides. BAF45D and BAF GEE/EDC labeling experiments are listed side by side for comparison. E337 and D340 could not be differentiated. ND indicates where residue-level quantitation could not be determined. (F) Tandem PHD domain of BAF45D (PBD 5VDC, white) was superimposed (rmsd = 1.3 Å) on the MOZ tandem PHD cocrystallized with a H3K14Cr peptide (PDB 5B76, green) to provide a model for peptide binding to BAF45D. Most protected residues (blue sticks) of BAF45D face toward the H3K14Cr peptide within adequate proximity (<4.5 Å) to generate a potential hydrogen bond (dashed lines). Asp and Glu residues were GEE/EDC labeled but remain unchanged after the addition of the H3K14Cr peptide (gray sticks), largely point away from the H3K14Cr peptide or are far removed (>6 Å) from its modeled binding site.

https://doi.org/10.1021/acsbiomedchemau.4c00009
ACS Bio Med Chem Au 2024, 4, 204−213

strong affinity for the crotonylated version of this peptide (H3K14Cr). To recapitulate these findings, we expressed and purified a biotinylated BAF45D$_{DPF}$ construct for AlphaLISA binding studies with Flag-tagged H3K14Cr peptide (Figure 1A). BAF45D$_{DPF}$ bound H3K14Cr with a K_d of 2.41 ± 0.5 nM, n = 3 (Figure 1B), which is consistent with prior studies and supports the use of this isolated system for initial footprinting experiments.

BAF45D$_{DPF}$ was prepared at 10 μM ± 50 μM of H3K14Cr peptide, labeled by 240 mM GEE and 8 mM EDC over a time course from 0 to 6.5 min followed by tryptic digestion and LC−MS/MS. GEE labeling introduces a stable side-chain modification onto Asp and Glu residues, resulting in a mass shift of +85.0527 Da. Seven of the nine tryptic peptides derived from BAF45D$_{DPF}$, including one missed cleavage, contain Asp or Glu residues as potential probes (Table S1). Modification rate constants (Kfp) were measured for the 6 fully tryptic peptides (Figure 1C, n = 1). Although the data presented are a lone replicate with multiple-time exposure points each, other experiments with different molar ratios demonstrated reproducible modification for both free BAF45D$_{DPF}$ and its complex with H3K14Cr peptide (Table S1, Figure S1, data not shown). The PR was calculated for all peptides as the fraction of Kfp$_{BAF45}$ over Kfp$_{BAF45\text{-}H3K14Cr}$.

Two sets of tryptic peptides comprise the PHD1 and PHD2 domains: residues 286-300/301-318 and 329-350/351-379, respectively, with a linker peptide 322-328 in between. Of the six labeled peptides, 329-350 and 322-328 had the highest protections (PR = 4.3 and 3.4). Peptide 286-300 has a PR of 1.4, indicating a more modest structural change relative to the other two peptides (Figure 1C). The three remaining peptides within BAF45D$_{DPF}$ showed minimal changes in modification rate (PR avg = 1.08). Peptide 301-318 contains neither Asp nor Glu and, therefore, cannot be labeled. Together, these data suggest that GEE footprinting is sufficiently specific and sensitive to detect recognition of histone tail modifications by the PHD readers in BAF and confirms the interactions in isolated BAF45D.

Protein Footprinting of Endogenous Canonical Full BAF Complex Binding to H3K14cr

Isolated BAF45D$_{DPF}$ domains (Figure 1B,C) exhibit specific and mechanistically plausible crotonylamide recognition,[14] but such binding experiments lack the context of the individual protein within its obligate complex, including any conformational changes. In addition, canonical BAF (∼1 MDa) contains 10−12 characterized subunits,[4,17] several of which contain histone mark recognition domains.[10,11] It remains unclear if BAF45D is the primary and/or sole subunit capable of binding to crotonyl lysine. To address this, we purified BAF complexes from HEK293T cells expressing Flag-BAF45D (Flag-BAF).[4] Our isolated, fully formed, canonical BAF complexes contain all known relevant subunits (BRM, ARID1A/B, BAF60, BAF170/155, BAF47, BAF57, ACTIN, ACTL6A, BCL7, and SS18) (Figure 2A). Flag-BAF crotonylamide recognition was measured by AlphaLISA using biotinylated-H3K14Cr peptide (Figure 2B). Flag-BAF bound H3K14Cr with a K_d of 8.61 ± 0.5 nM, n = 3, suggesting that BAF45D binds to crotonylamide groups within BAF and further recapitulating analyses with BAF45D$_{DPF}$[14] (Figure 1B,C).

To further assess the H3K14Cr peptide−BAF interaction, protein footprinting studies for Flag-BAF were executed as described above for BAF45D$_{DPF}$. Initial screening analysis was carried out with a single 5 min time point using ProtMap software that allowed the identification and quantification of peptide modifications in an automated mode,[34] followed by manual validation for peptides that met the screening threshold, which was a PR value of ≥1.3. Taking inputs of LC−MS data, BAF sequence, type of enzyme used, and modification mass, ProtMap identified over 630 tryptic peptides across Flag-BAF, with an average protein sequence coverage of ∼63%. ProtMap, at the same time, revealed the sites of GEE labeling for 177 of the 630 peptides that were found to be reproducibly modified by GEE for both Flag-BAF and Flag-BAF/H3K14Cr peptide samples. The distribution of PR values for all labeled peptides within Flag-BAF (Figure 2C) ranged from 0.04 to 1.68 with identical mean and median values of 0.96, indicating (consistent with our stated hypothesis) that most peptides (>90%) exhibit similar labeling across Flag-BAF regardless of H3K14Cr peptide binding. The peptides with PR significantly less than 1 likely indicate regions experiencing significant allosteric changes associated with histone reader functions; however, the analysis of these data is beyond the scope of this paper. Sixteen peptides identified with PR of ≥1.3 (localized to subunits: ARID1A, ACTL6A, ACTIN, BCL7, BRM, BAF170 and BAF45D) were manually analyzed using data from all three time points. These analyses revealed four peptides with consistent and significant PR of ≥1.3 and one peptide trending with PR = 1.24 in both ProtMap and manual analysis, where three reside within BAF45D and two within BRM. These data suggest that BAF45D and BRM are the primary BAF subunits responsive to H3K14Cr peptide binding.

We calculated Kfp for all peptides within BAF45D and BRM ± H3K14Cr peptide (Tables S3 and S5, Figure S2). The three most protected peptides are 286-300 (PHD1), 322-328 (PHD2), and 329-350 (PHD2) (Figure 2D). These peptides within BAF45D in BAF are identical to the three most protected peptides in BAF45D$_{DPF}$, demonstrating the conservation of mechanism and structure effects of lysine crotonylation binding when BAF45D is positioned within the full BAF complex. Furthermore, BRM contained two protected peptides, 953-961 within the linker between the NRecA and CRecA lobes and 1435-1444 in the bromodomain. These data are the first to indicate that BRM may be directly influenced by crotonyl lysine binding on histone 3 tails.

Single Residue Analysis of Specific Residues within BAF45D Bind to the H3K14Cr Peptide

We further analyzed the footprinting data to identify the specific side chains sensitive to H3K14Cr binding within BAF45D$_{DPF}$ (Figures 2E, S1 and Table S2). There are 18 Asp and Glu residues, 14 of which are localized to PHD1 and PHD2. We observed 5 residues that were sensitive to H3K14Cr peptide binding to BAF45D$_{DPF}$ (Figure 2E). Asp274 is not located directly within the PHD1 or PHD2 pockets but is <4.5 Å from the crotonylamide group (Figure 2F). Asp274 exhibited a significant decrease (2.37, Figure 2E) in labeling in the presence of the H3K14Cr peptide despite a lack of change in the modification rate constant for its containing peptide (261-281; Figure 2D). For peptides 286-300 (PHD1), Asp297 showed a modest decrease in modification rate constant (1.4), while Glu291 exhibited no change, and Glu290 was not detected. The linker peptide 322-328 contains only one Glu residue, thus requiring no additional analysis. Peptide 329-350 contains 6 potential sites of GEE labeling, 3 of which encompass the PHD2 pocket (Asp346, Asp347, Asp349), while the other 3 (Glu337,

https://doi.org/10.1021/acsbiomedchemau.4c00009
ACS Bio Med Chem Au 2024, 4, 204−213

A.

Location	Sequence BAF45D within BRM	Protection Ratio
195-209	GQPLPETLQLAVQGK	0.67
334-346	PQGLDPVEILQER	1.05
403-413	DTTLETALNSK	0.89
448-460	HQEYLNSILQHAK	1.12
479-489	AVATWHANTER	0.95
506-516	LMAEDEEGYRK	0.85
565-596	KAEENAEGGESALGPDGE PIDESSQMSDLPVK	0.63
605-613	VLFGPEAPK	1.08
660-672	ILLDPNSEEVSEK	0.97
924-936	VDLNEEETILIIR	0.89
953-961	**EVESQLPEK**	**1.73**
985-994	GILLTDGSEK	1.16
1246-1255	REEEFDLFMR	1.00
1274-1286	LMEEDELPSWIIK	0.97
1313-1323	DVDYSDALTEK	1.11
1328-1342	AIEDGNLEEMEEEVR	0.92
1422-1433	QLSEVFIQLPSR	0.85
1435-1444	**ELPEYYELIR**	**1.29**

C.

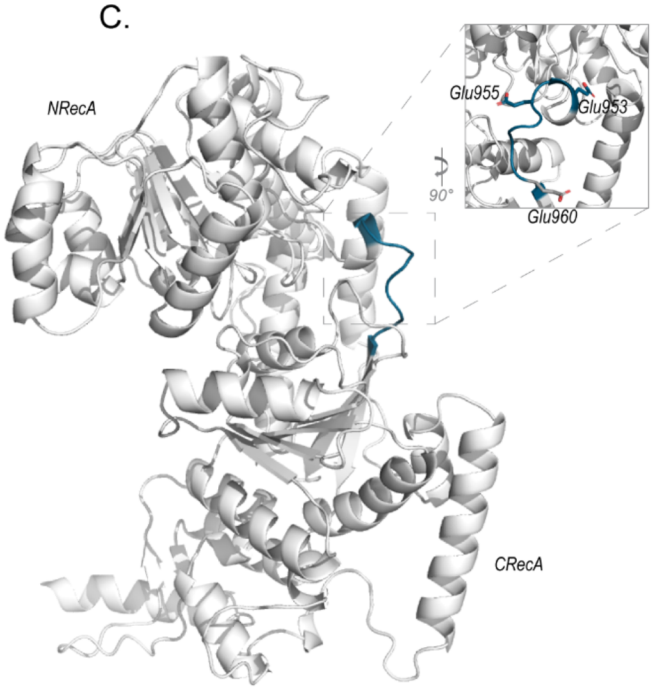

B.

Location	Residue level Modification	Protection Ratio
953-961	E953	1.67
	E955	1.58
	E960	0.94
1435-1444	E1435	1.30
	E1438	1.25
	E1441	ND

D.

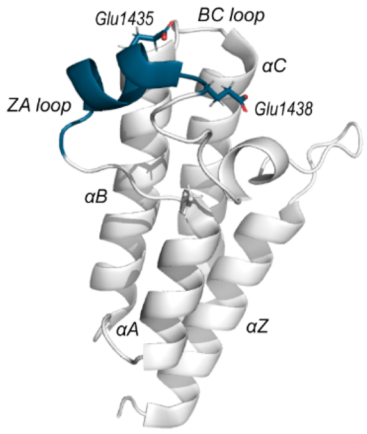

E.

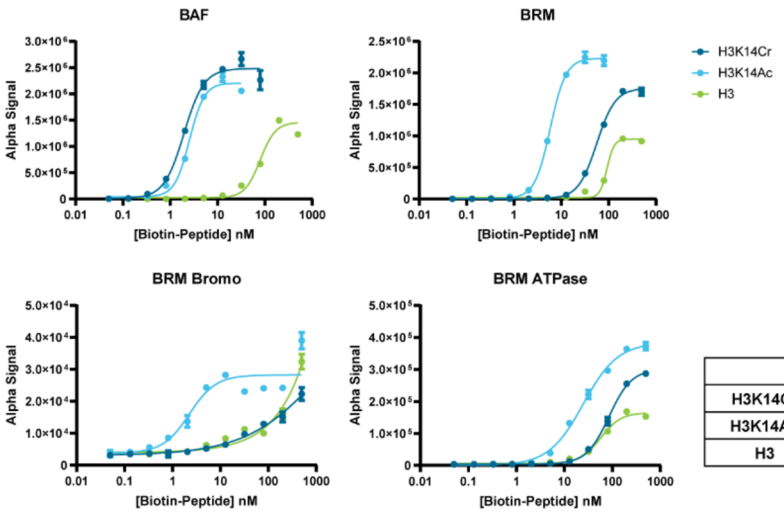

	BAF	BRM	BRM Bromo	BRM ATPase
H3K14Cr	2.22 ± 0.38	46.19 ± 14.38	ND	87.11 ± 2.28
H3K14Ac	4.32 ± 2.50	5.97 ± 0.14	ND	31.75 ± 9.82
H3	92.63 ± 18.21	90.23 ± 3.88	ND	54.93 ± 2.89

Figure 3. H3K14Cr (in)directly modulates BRM ATPase. Footprinting with BAF revealed protections within the bromo and ATPase domains of BAF. (A) Table of the PR for BRM peptides following GEE/EDC labeling of Flag-BAF where protected peptides are in bold. (B) Table of the PR for each Asp and Glu residue located within protected peptides. ND indicates where residue-level quantitation could not be determined. (C) Predicted BRM structure (AF-P51531-F1-model_v1) showing the NRecA and CRecA lobes. Protected peptide 953-961 (blue) lies between the RecA lobes within the hinge region. (D) Bromodomain of BRM showing the canonical four-helix bundle (PDB 6HAZ). Protected peptide 1435-1444 (blue) lies within the ZA loop at the opening of the bromodomain pocket. (E) AlphaLISA was used to assess Flag-tagged BAF, full-length BRM, BRM bromodomain, and BRM ATPase domain binding to H3 peptide in the presence of crotonyl (H3K14Cr; blue), acetyl (H3K14Ac; light blue), or no (H3K14; green) lysine modifications. The table contains the K_d for each binding pair (mean ± SD; n = 2).

Asp339, Asp340) are distally located. Upon residue-level analysis, we detected minor changes in solvent accessibility for the distal sites (1.28-Glu337/Asp340, which are derived from the same peak and 1.34-Asp339). Interestingly, Asp346 and

https://doi.org/10.1021/acsbiomedchemau.4c00009
ACS Bio Med Chem Au 2024, 4, 204−213

Asp349 exhibited significantly decreased modification rate constants (5.22 and 6.51, respectively), whereas Asp347, flanked by the aforementioned residues, lacked any change. A similar analysis was performed for the BAF45D residues within BAF (Figures 2E, S2 and Table S4). With the exception of Asp274, we observed comparable results to BAF45D$_{DPF}$, albeit with a smaller magnitude of change in modification rates. This discrepancy is likely due to a combination of the increased complexity of a 1 MDa, multisubunit complex (Flag-BAF) as compared to an isolated domain (BAF45D$_{DPF}$) as well as differences in protein concentrations and heterogeneity between the two types of experiments.

Modeling of BAF45D Binding to H3K14Cr Peptide is Supported by Protected Residues

We generated a model for peptide binding to BAF45D (Figure 2F) using the previously deposited structures by Xiong et al.[14] The tandem PHD domain of BAF45D (PBD 5VDC, white) was superimposed (rmsd = 1.3 Å) on the MOZ tandem PHD domain cocrystallized with a H3K14Cr peptide (PDB 5B76, green) to provide a model for peptide binding to BAF45D. Most protected residues (blue sticks) of BAF45D face toward the H3K14Cr peptide within adequate proximity (<4.5 Å) to generate a potential hydrogen bond (dashed lines). This includes Asp274 near the crotonylamide group and Glu326 adjacent to Arg8′. Asp and Glu residues that were labeled but remain unchanged after the addition of the H3K14Cr peptide (gray sticks) largely point away from the H3K14Cr peptide or are far removed (>6 Å) from its modeled binding site. The specificity is highlighted by the labeling seen for sequential residues Asp346, Asp347, and Asp349. Here, the protected residues Asp346 and Asp349 have side chains that point toward H3K14Cr and are within a range to generate hydrogen bonds with Arg2′ (Figure 2F, inset). In contrast, the side chain of Asp347 points away, positioning itself out of range for bonding clearly explaining the lack of protection during labeling (Figure 2E,F).

H3 Peptide Binds to BRM Irrespective of Crotonylation Status

H3K14Cr peptide binding to Flag-BAF produced two protected BRM peptides, located in the ATPase module and bromodomain (Figure 3A and Table S5). No crystal structure for the full BRM protein has been reported. Thus, for structural analysis of the BRM-protected peptide within the ATPase, we used the AlphaFold predicted structure (AF-P51531-F1-model_v1) (Figure 3C).[35,36] While AF2 structures are imperfect, especially at residue-level resolution, in the protected peptide region, AF-P51531 aligned well with the nucleosome bound form of BRG1 from the recent high-resolution cryoEM structure of canonical BAF,[16] the isolated ATPase and SnAC domains of BRM, (PDB 6EG2),[37] as well as the homologous Snf2 (T. thermophilus; PDB 5HZR).[38] The protected peptide, 953-961, lies distal from the nucleosome between the NRecA and CRecA lobes of BRM in a structurally flexible region. Glu953 and Glu955 are the residues primarily affected by H3K14Cr binding (Figure 3C, inset), which was recapitulated in subsequent experiments at a 1:10 BAF:H3K14Cr ratio (data not shown). The side chains of Glu953 and Glu955 are located on opposite sides of a loop, stretching into the NRecA lobe (Figure 3C inset, blue). Interestingly, the nearby side chain of Glu960 is solvent-facing (Figure 3C inset, gray) but does not appear to contribute significantly to the protected labeling.

To evaluate the second protected peptide, we used a published, high-resolution crystal structure of the bromodomain of BRM (PDB 6HAZ)[39] as shown in Figure 3D. Bromodomain structures are composed of four helices (αA, αB, αC, and αZ) arranged into a left-handed bundle interspersed by ZA and BC loops.[40] This orientation creates a hydrophobic pocket that is capable of recognizing lysine modifications on histone tails, including acetylation and crotonylation.[10,41,42] Modestly protected peptide 1435-1444 lies within the ZA loop in between the αA and αZ helices, located near the opening of the bromodomain pocket (Figure 3D), where the side chains of the protected residues, Glu1435 and Glu1438, face inward (Figure 3B,D).

The orientation of protected residues within BRM suggests a potential interaction with H3K14Cr. We next assessed the direct binding and the effect of crotonylation by AlphaLISA assay, including noncrotonylated (H3K14) and acetylated (H3K14Ac) peptide controls (Figure 3E). We observed that BAF binds to unmodified H3 peptide, with increased affinity in the presence of modified lysine residues (Ac ≈ Cr ≫H3). Full-length BRM also binds H3 peptide, with enhanced affinity for marked lysines (Ac ≫ Cr > H3). When assessing direct binding to the domains of BRM, we were unable to observe the binding of any H3 peptide to the bromodomain. However, we observed that the ATPase binds all three peptides, where H3K14Cr binds with the same affinity as H3 (Ac > Cr ≈ H3). Together, these data suggest that BRM binds H3 histone tails irrespective of crotonylation status and that these binding events are primarily localized to the ATPase region.

DISCUSSION

Using protein footprinting, we provided a detailed map of modified histone tail interactions in the context of the full BAF complex, localizing H3K14Cr peptide binding to the DPF domain of BAF45D (Figure 2D,E), as well as effects in both the bromodomain and ATPase module of BRM (Figure 3A,B). These data are validated by footprinting studies of BAF45D$_{DPF}$, which showed equivalent peptide and residue-level protections within the PHD1, PHD2, and linker regions. Structural modeling supports these data, highlighting Asp and Glu residues that are in the correct position to interact with an H3K14Cr peptide. Together, these data provide a novel framework for interpreting BAF reader functions.

BAF45D interacts with modified histone tails in a bipartite fashion, via hydrophobic interactions in PHD1 and electrostatic interactions in PHD2. The hydrophobic pocket of PHD1 includes Phe275, Leu307, and Trp322 that engage with K14Cr.[14,15] The presence of Gly302, lacking a side chain, allows for the tight insertion of the long, planar, crotonylamide group into the PHD1 pocket and likely contributes to enhanced affinity compared to other acyl groups.[14] Studies using alternative chemistries like hydroxyl radical footprinting are ideal for assessing residues of this type. Unfortunately, the scavenging by such a large protein complex provides challenges for OH labeling methods. Although GEE/EDC labeling does not address these hydrophobic residues, we were able to observe protections in nearby residues, Asp274 and Asp297 (Figure 2E). The BAF45D$_{DPF}$-MOZ superimposed model shows that these residues are in close proximity to the K14Cr (<6 Å), suggesting that the observed protections are due to K14Cr insertion into the PHD1 pocket (Figure 2E,F). The negatively charged patch within PHD2 contains many Asp and Glu residues contributing to the electrostatic interaction between BAF45D and the histone

https://doi.org/10.1021/acsbiomedchemau.4c00009
ACS Bio Med Chem Au 2024, 4, 204−213

tail.[14,15] Notably, Glu326 and Asp346 have been reported to interact with H3 Lys4 and Arg2, respectively, where mutations in the latter contribute to a disruption in histone tail peptide recognition.[15] Asp346 and Asp349 face the surface of the H3K14Cr peptide and are highly protected following binding (Figure 2E,F, blue). In contrast, we see no protection of Asp347, which points away from the H3K14Cr peptide (Figure 2E,F, gray). Again, modeled BAF45D$_{DPF}$-MOZ reveals the nature of these protections, where Asp346 and Asp349 are 3.3 and 1.8 Å, respectively, from H3 Arg2′, whereas Asp347 is >8 Å away.

In this study, we also characterized the strength of binding of histone 3 tail peptides to BAF45D$_{DPF}$ and the full BAF complex. The Kds we measured for isolated DPF domains are lower (~2.5−33.0 nM, Figures 1B, 2B, and 3E) than what has been previously reported (0.085−1.0 μM),[14,15] which may be due to differences in assay format (ITC vs AlphaLISA) and/or to saturation issues causing a slight hook effect in the AlphaLISA assay. We also observe that BAF binds unmodified H3K14 peptide, which is enhanced in the presence of crotonylation (Figure 3E). Earlier work has demonstrated that lysine mark recognition domains, including those found in chromatin remodelers, bind to unmodified histone tails, where acetyl-/acylation functions to enhance binding affinities and promote the interaction.[14,43−45] DPF domains play a critical role in these binding events, where mutations in either PHD1 or PHD2 domains result in diminished histone tail binding.[15]

Footprinting data also exposed conformational effects to H3 tail peptides within BRM, with changes in both the ATPase- and bromodomains (Figure 3A−D). Direct binding assays indicated that the ATPase is primarily responsible for H3 binding within BRM (Figure 3E), whereas changes in the bromodomain are likely attributable to conformational rearrangements. These data are somewhat surprising given the well-characterized nature of bromodomain recognition of marked lysines on histone tails, including those of BRM and BRG.[10,42,46,47] It is possible that our AlphaLISA assay is not capable of capturing the BRM bromodomain−H3 interaction, and additional studies using methods that yield full thermodynamic binding parameters may be required. Although ATPase binding to histone tails is less well-understood, recent structural characterization of BAF in complex with a mononucleosome provides a hypothesis and potential model for the interaction,[17] where the ATPase module contains a "nucleosome recruitment" region that recognizes and binds histone tails in order to initiate chromatin remodeling.

CONCLUSIONS

Mass spectrometry-based protein footprinting provided a detailed map of H3K14Cr histone tail interactions in the context of the full BAF chromatin remodeling complex. The data localized binding to key residues in the PHD1 and PHD2 domains of BAF45D, consistent with experiments performed on the isolated DPF domain, and revealed potential conformational changes in the ATPase and bromodomain of BRM. Integrating footprinting results with structural modeling and binding assays elucidated the molecular basis for crotonylamide recognition by BAF45D. Furthermore, the novel finding of direct histone tail engagement by the BRM ATPase suggests additional mechanisms for BAF recruitment and chromatin remodeling. This study illustrates the power of footprinting methods to map binding interfaces in large, multisubunit complexes and provides new insights into BAF reader functions.

ASSOCIATED CONTENT

Supporting Information

The Supporting Information is available free of charge at https://pubs.acs.org/doi/10.1021/acsbiomedchemau.4c00009.

Excel sheet includes protection ratio calculations and analysis for all BAF subunit peptides at 5 min H3K14Cr treatment time point (XLSX)

Figures and tables describe the modification rates and rate constants for the peptides and residues affected by H3K14Cr treatment (PDF)

AUTHOR INFORMATION

Corresponding Authors

Mark R. Chance − *NeoProteomics, Moreland Hills, Ohio 44022, United States; Center for Proteomics and Bioinformatics, Department of Nutrition, Case Western Reserve University, Cleveland, Ohio 44106, United States;* orcid.org/0000-0002-2991-6405; Email: mrc16@case.edu

Steve Bellon − *Foghorn Therapeutics, Cambridge, Massachusetts 02139, United States*; Email: sbellon@foghorntx.com

Authors

Marissa R. Martinez − *Foghorn Therapeutics, Cambridge, Massachusetts 02139, United States;* Present Address: Covant Therapeutics, Boston, Massachusetts 02108, United States

Janna Kiselar − *NeoProteomics, Moreland Hills, Ohio 44022, United States; Center for Proteomics and Bioinformatics, Department of Nutrition, Case Western Reserve University, Cleveland, Ohio 44106, United States*

Benlian Wang − *Center for Proteomics and Bioinformatics, Department of Nutrition, Case Western Reserve University, Cleveland, Ohio 44106, United States*

Dipti Sadalge − *Foghorn Therapeutics, Cambridge, Massachusetts 02139, United States*

Laura Zawadzke − *Foghorn Therapeutics, Cambridge, Massachusetts 02139, United States;* Present Address: LifeMine Therapeutics, Cambridge, Massachusetts 02114, United States.

Asad Taherbhoy − *Foghorn Therapeutics, Cambridge, Massachusetts 02139, United States*

Derek Musser − *Foghorn Therapeutics, Cambridge, Massachusetts 02139, United States*

Yunji Davenport − *Foghorn Therapeutics, Cambridge, Massachusetts 02139, United States*

Jeremy Setser − *Foghorn Therapeutics, Cambridge, Massachusetts 02139, United States;* Present Address: Flare Therapeutics, Cambridge, Massachusetts 02114, United States.; orcid.org/0000-0002-2032-6740

Complete contact information is available at: https://pubs.acs.org/10.1021/acsbiomedchemau.4c00009

Author Contributions

[▽]M.R.M. and J.K. contributed equally to this work. The manuscript was written through contributions of all authors. All authors have given approval to the final version of the manuscript. CRediT: **Marissa R. Martinez** conceptualization, data curation, formal analysis, investigation, methodology,

https://doi.org/10.1021/acsbiomedchemau.4c00009
ACS Bio Med Chem Au 2024, 4, 204−213

project administration, validation, visualization, writing-original draft, writing-review & editing; **Janna Kiselar** conceptualization, data curation, formal analysis, investigation, methodology, project administration, resources, supervision, validation, visualization, writing-original draft, writing-review & editing; **Benlian Wang** data curation, formal analysis, investigation, methodology, validation; **Dipti Sadalge** data curation, formal analysis, investigation, methodology, visualization, writing-original draft; **Laura Zawadzke** data curation, formal analysis, methodology, supervision; **Asad Taherbhoy** supervision; **Derek Musser** data curation, formal analysis, investigation, methodology, visualization, writing-original draft; **Yunji Davenport** supervision; **Jeremy W. Setser** conceptualization, data curation, formal analysis, investigation, methodology, project administration, visualization, writing-review & editing; **Mark R. Chance** conceptualization, methodology, project administration, validation, visualization, writing-original draft, writing-review & editing; **Steven F. Bellon** conceptualization, project administration, resources, supervision.

Notes

The authors declare the following competing financial interest(s): The following own FHT stock (M.R.M., J.S., M.R.C., D.S., L.Z., A.T., D.M., Y.D., S.B.) or were compensated as part of this research through a subcontract to the FHT vendor, Neo Proteomics, Inc. (M.R.C., J.K.). Marissa Martinez (owns FHT stock)-former Foghorn employee; Jeremy Setser (owns FHT stock)-former Foghorn employee; Janna Kiselar (consultant for FHT sub-contractor, Neo Proteomics, Inc.; Mark R. Chance (owns FHT stock, consultant for FHT sub-contractor, Neo Proteomics, Inc.).

■ ABBREVIATIONS

BAF, BRG-/BRM-associated factor; $BAF45D_{DPF}$, isolated DPF domain of BAF45D; DPF, double PHD; H3K14, 25-mer histone tail peptide; H3K14Cr, crotonylated histone 3 peptide; LC−MS, liquid chromatography−mass spectrometry; MOZ, monocytic leukemic zinc finger protein; MORF, MOZ-related factor; MOZ_{DPF}, isolated DPF domains of MOZ; PHD, plant homeodomain; PHD1, first PHD finger domain; PHD2, second PHD finger domain; PR, protection ratio

■ REFERENCES

(1) Hyun, K.; Jeon, J.; Park, K.; Kim, J. Writing, Erasing and Reading Histone Lysine Methylations. *Exp. Mol. Med.* **2017**, *49* (4), No. e324.

(2) Topal, S.; Vasseur, P.; Radman-Livaja, M.; Peterson, C. L. Distinct Transcriptional Roles for Histone H3-K56 Acetylation during the Cell Cycle in Yeast. *Nat. Commun.* **2019**, *10* (1), No. 4372, DOI: 10.1038/s41467-019-12400-5.

(3) Tan, M.; Luo, H.; Lee, S.; Jin, F.; Yang, J. S.; Montellier, E.; Buchou, T.; Cheng, Z.; Rousseaux, S.; Rajagopal, N.; Lu, Z.; Ye, Z.; Zhu, Q.; Wysocka, J.; Ye, Y.; Khochbin, S.; Ren, B.; Zhao, Y. Identification of 67 Histone Marks and Histone Lysine Crotonylation as a New Type of Histone Modification. *Cell* **2011**, *146* (6), 1016−1028.

(4) Mashtalir, N.; D'Avino, A. R.; Michel, B. C.; Luo, J.; Pan, J.; Otto, J. E.; Zullow, H. J.; McKenzie, Z. M.; Kubiak, R. L.; St Pierre, R.; Valencia, A. M.; Poynter, S. J.; Cassel, S. H.; Ranish, J. A.; Kadoch, C. Modular Organization and Assembly of SWI/SNF Family Chromatin Remodeling Complexes. *Cell* **2018**, *175* (5), 1272−1288.e20.

(5) McBride, M. J.; Pulice, J. L.; Beird, H. C.; Ingram, D. R.; D'Avino, A. R.; Shern, J. F.; Charville, G. W.; Hornick, J. L.; Nakayama, R. T.; Garcia-Rivera, E. M.; Araujo, D. M.; Wang, W. L.; Tsai, J. W.; Yeagley, M.; Wagner, A. J.; Futreal, P. A.; Khan, J.; Lazar, A. J.; Kadoch, C. The SS18-SSX Fusion Oncoprotein Hijacks BAF Complex Targeting and Function to Drive Synovial Sarcoma. *Cancer Cell* **2018**, *33* (6), 1128−1141.e7.

(6) Wilson, B. G.; Helming, K. C.; Wang, X.; Kim, Y.; Vazquez, F.; Jagani, Z.; Hahn, W. C.; Roberts, C. W. M. Residual Complexes Containing SMARCA2 (BRM) Underlie the Oncogenic Drive of SMARCA4 (BRG1) Mutation. *Mol. Cell. Biol.* **2014**, *34* (6), 1136−1144.

(7) Wanior, M.; Krämer, A.; Knapp, S.; Joerger, A. C. Exploiting Vulnerabilities of SWI/SNF Chromatin Remodelling Complexes for Cancer Therapy. *Oncogene* **2021**, *40* (21), 3637−3654, DOI: 10.1038/s41388-021-01781-x.

(8) Strahl, B. D.; Allis, C. D. The Language of Covalent Histone Modifications. *Nature* **2000**, *403* (6765), 41−45.

(9) Wang, W.; Chi, T.; Xue, Y.; Zhou, S.; Kuo, A.; Crabtree, G. R. Architectural DNA Binding by a High-Mobility-Group/Kinesin-like Subunit in Mammalian SWI/SNF-Related Complexes. *Proc. Natl. Acad. Sci. U.S.A.* **1998**, *95* (2), 492−498.

(10) Filippakopoulos, P.; Picaud, S.; Mangos, M.; Keates, T.; Lambert, J. P.; Barsyte-Lovejoy, D.; Felletar, I.; Volkmer, R.; Müller, S.; Pawson, T.; Gingras, A. C.; Arrowsmith, C. H.; Knapp, S. Histone Recognition and Large-Scale Structural Analysis of the Human Bromodomain Family. *Cell* **2012**, *149* (1), 214−231.

(11) Allen, M. D.; Freund, S. M. V.; Bycroft, M.; Zinzalla, G. SWI/SNF Subunit BAF155 N-Terminus Structure Informs the Impact of Cancer-Associated Mutations and Reveals a Potential Drug Binding Site. *Commun. Biol.* **2021**, *4* (1), No. 528.

(12) Sabari, B. R.; Zhang, D.; Allis, C. D.; Zhao, Y. Metabolic Regulation of Gene Expression through Histone Acylations. *Nat. Rev. Mol. Cell Biol.* **2017**, *18* (2), 90−101, DOI: 10.1038/nrm.2016.140.

(13) Musselman, C. A.; Lalonde, M. E.; Côté, J.; Kutateladze, T. G. Perceiving the Epigenetic Landscape through Histone Readers. *Nat. Struct. Mol. Biol.* **2012**, *19*, 1218−1227.

(14) Xiong, X.; Panchenko, T.; Yang, S.; Zhao, S.; Yan, P.; Zhang, W.; Xie, W.; Li, Y.; Zhao, Y.; Allis, C. D.; Li, H. Selective Recognition of Histone Crotonylation by Double PHD Fingers of MOZ and DPF2. *Nat. Chem. Biol.* **2016**, *12* (12), 1111−1118.

(15) Huber, F. M.; Greenblatt, S. M.; Davenport, A. M.; Martinez, C.; Xu, Y.; Vu, L. P.; Nimer, S. D.; Hoelz, A. Histone-Binding of DPF2Mediates Its Repressive Role in Myeloid Differentiation. *Proc. Natl. Acad. Sci. U.S.A.* **2017**, *114* (23), 6016−6021.

(16) He, S.; Wu, Z.; Tian, Y.; Yu, Z.; Yu, J.; Wang, X.; Li, J.; Liu, B.; Xu, Y. Structure of Nucleosome-Bound Human BAF Complex. *Science* **2020**, *367* (6480), 875−881.

(17) Mashtalir, N.; Suzuki, H.; Farrell, D. P.; Sankar, A.; Luo, J.; Filipovski, M.; D'Avino, A. R.; Pierre, R., St; Valencia, A. M.; Onikubo, T.; Roeder, R. G.; Han, Y.; He, Y.; Ranish, J. A.; DiMaio, F.; Walz, T.; Kadoch, C. A Structural Model of the Endogenous Human BAF Complex Informs Disease Mechanisms. *Cell* **2020**, *183* (3), 802−817.e24.

(18) Soshnikova, N. V.; Sheynov, A.; Tatarskiy, Ev.; Georgieva, S. G. The DPF Domain As a Unique Structural Unit Participating in Transcriptional Activation, Cell Differentiation, and Malignant Transformation. *Acta Nat.* **2020**, *12*, 57−65.

(19) Wang, L.; Chance, M. R. Protein Footprinting Comes of Age: Mass Spectrometry for Biophysical Structure Assessment. *Mol. Cell. Proteomics* **2017**, 706−716, DOI: 10.1074/mcp.O116.064386.

(20) Kiselar, J.; Chance, M. R. High-Resolution Hydroxyl Radical Protein Footprinting: Biophysics Tool for Drug Discovery. *Annu. Rev. Biophys* **2018**, *47*, 315−333.

(21) Goodwin, J. M.; Walkup, W. G.; Hooper, K.; Li, T.; Kishi-Itakura, C.; Ng, A.; Lehmberg, T.; Jha, A.; Kommineni, S.; Fletcher, K.; Garcia-Fortanet, J.; Fan, Y.; Tang, Q.; Wei, M.; Agrawal, A.; Budhe, S. R.; Rouduri, S. R.; Baird, D.; Saunders, J.; Kiselar, J.; Chance, M. R.; Ballabio, A.; Appleton, B. A.; Brumell, J. H.; Florey, O.; Murphy, L. O. GABARAP Sequesters the FLCN-FNIP Tumor Suppressor Complex to Couple Autophagy with Lysosomal Biogenesis. *Sci. Adv.* **2021**, *7* (40), No. eabj2485.

https://doi.org/10.1021/acsbiomedchemau.4c00009
ACS Bio Med Chem Au 2024, 4, 204−213

(22) Chance, M. R.; Farquhar, E. R.; Yang, S.; Lodowski, D. T.; Kiselar, J. Protein Footprinting: Auxiliary Engine to Power the Structural Biology Revolution. *J. Mol. Biol.* **2020**, *432* (9), 2973−2984.
(23) Xu, G.; Chance, M. R. Hydroxyl Radical-Mediated Modification of Proteins as Probes for Structural Proteomics. *Chem. Rev.* **2007**, *107* (8), 3514−3543.
(24) Gau, B.; Garai, K.; Frieden, C.; Gross, M. L. Mass Spectrometry-Based Protein Footprinting Characterizes the Structures of Oligomeric Apolipoprotein E2, E3, and E4. *Biochemistry* **2011**, *50* (38), 8117−8126.
(25) Zhang, H.; Wen, J.; Huang, R. Y.-C.; Blankenship, R. E.; Gross, M. L. Mass Spectrometry-Based Carboxyl Footprinting of Proteins: Method Evaluation. *Int. J. Mass Spectrom.* **2012**, *312*, 78−86.
(26) Hoare, D. G.; Olson, A.; Koshland, D. E. The Reaction of Hydroxamic Acids with Water-Soluble Carbodiimides. A Lossen Rearrangement. *J. Am. Chem. Soc.* **1968**, *90* (6), 1638−1643.
(27) Sharp, J. S.; Becker, J. M.; Hettich, R. L. Analysis of Protein Solvent Accessible Surfaces by Photochemical Oxidation and Mass Spectrometry. *Anal. Chem.* **2004**, *76* (3), 672−683.
(28) Zhang, H.; Shen, W.; Rempel, D.; Monsey, J.; Vidavsky, I.; Gross, M. L.; Bose, R. Carboxyl-Group Footprinting Maps the Dimerization Interface and Phosphorylation-Induced Conformational Changes of a Membrane-Associated Tyrosine Kinase. *Mol. Cell. Proteomics* **2011**, *10* (6), No. M110.005678, DOI: 10.1074/mcp.M110.005678.
(29) Maleknia, S. D.; Kiselar, J. G.; Downard, K. M. Hydroxyl Radical Probe of the Surface of Lysozyme by Synchrotron Radiolysis and Mass Spectrometry. *Rapid Commun. Mass Spectrom.* **2002**, *16* (1), 53−61.
(30) Yan, Y.; Chen, G.; Wei, H.; Huang, R. Y. C.; Mo, J.; Rempel, D. L.; Tymiak, A. A.; Gross, M. L. Fast Photochemical Oxidation of Proteins (FPOP) Maps the Epitope of EGFR Binding to Adnectin. *J. Am. Soc. Mass Spectrom.* **2014**, *25* (12), 2084−2092.
(31) Chance, M. R.; Sclavi, B.; Woodson, S. A.; Brenowitz, M. Examining the Conformational Dynamics of Macromolecules with Time-Resolved Synchrotron X-Ray "Footprinting. *Structure* **1997**, *5*, 865−869.
(32) Wiśniewski, J. R. Filter-Aided Sample Preparation for Proteome Analysis. *Methods Mol. Biol.* **2018**, *1841*, 3−10.
(33) Kaur, P.; Tomechko, S. E.; Kiselar, J.; Shi, W.; Deperalta, G.; Wecksler, A. T.; Gokulrangan, G.; Ling, V.; Chance, M. R. Characterizing Monoclonal Antibody Structure by Carboxyl Group Footprinting. *MAbs* **2015**, *7* (3), 540−552.
(34) Kaur, P.; Kiselar, J. G.; Chance, M. R. Integrated Algorithms for High-Throughput Examination of Covalently Labeled Biomolecules by Structural Mass Spectrometry. *Anal. Chem.* **2009**, *81* (19), 8141−8149.
(35) Jumper, J.; Evans, R.; Pritzel, A.; Green, T.; Figurnov, M.; Ronneberger, O.; Tunyasuvunakool, K.; Bates, R.; Žídek, A.; Potapenko, A.; Bridgland, A.; Meyer, C.; Kohl, S. A. A.; Ballard, A. J.; Cowie, A.; Romera-Paredes, B.; Nikolov, S.; Jain, R.; Adler, J.; Back, T.; Petersen, S.; Reiman, D.; Clancy, E.; Zielinski, M.; Steinegger, M.; Pacholska, M.; Berghammer, T.; Bodenstein, S.; Silver, D.; Vinyals, O.; Senior, A. W.; Kavukcuoglu, K.; Kohli, P.; Hassabis, D. Highly Accurate Protein Structure Prediction with AlphaFold. *Nature* **2021**, *596* (7873), 583−589.
(36) Varadi, M.; Anyango, S.; Deshpande, M.; Nair, S.; Natassia, C.; Yordanova, G.; Yuan, D.; Stroe, O.; Wood, G.; Laydon, A.; Žídek, A.; Green, T.; Tunyasuvunakool, K.; Petersen, S.; Jumper, J.; Clancy, E.; Green, R.; Vora, A.; Lutfi, M.; Figurnov, M.; Cowie, A.; Hobbs, N.; Kohli, P.; Kleywegt, G.; Birney, E.; Hassabis, D.; Velankar, S. AlphaFold Protein Structure Database: Massively Expanding the Structural Coverage of Protein-Sequence Space with High-Accuracy Models. *Nucleic Acids Res.* **2022**, *50* (D1), D439−D444.
(37) Papillon, J. P. N.; Nakajima, K.; Adair, C. D.; Hempel, J.; Jouk, A. O.; Karki, R. G.; Mathieu, S.; Möbitz, H.; Ntaganda, R.; Smith, T.; Visser, M.; Hill, S. E.; Hurtado, F. K.; Chenail, G.; Bhang, H. E. C.; Bric, A.; Xiang, K.; Bushold, G.; Gilbert, T.; Vattay, A.; Dooley, J.; Costa, E. A.; Park, I.; Li, A.; Farley, D.; Lounkine, E.; Yue, Q. K.; Xie, X.; Zhu, X.; Kulathila, R.; King, D.; Hu, T.; Vulic, K.; Cantwell, J.; Luu, C.; Jagani, Z. Discovery of Orally Active Inhibitors of Brahma Homolog (BRM)/SMARCA2 ATPase Activity for the Treatment of Brahma Related Gene 1 (BRG1)/SMARCA4-Mutant Cancers. *J. Med. Chem.* **2018**, *61* (22), 10155−10172.
(38) Xia, X.; Liu, X.; Li, T.; Fang, X.; Chen, Z. Structure of Chromatin Remodeler Swi2/Snf2 in the Resting State. *Nat. Struct Mol. Biol.* **2016**, *23* (8), 722−729.
(39) Farnaby, W.; Koegl, M.; Roy, M. J.; Whitworth, C.; Diers, E.; Trainor, N.; Zollman, D.; Steurer, S.; Karolyi-Oezguer, J.; Riedmueller, C.; Gmaschitz, T.; Wachter, J.; Dank, C.; Galant, M.; Sharps, B.; Rumpel, K.; Traxler, E.; Gerstberger, T.; Schnitzer, R.; Petermann, O.; Greb, P.; Weinstabl, H.; Bader, G.; Zoephel, A.; Weiss-Puxbaum, A.; Ehrenhöfer-Wölfer, K.; Wöhrle, S.; Boehmelt, G.; Rinnenthal, J.; Arnhof, H.; Wiechens, N.; Wu, M.-Y.; Owen-Hughes, T.; Ettmayer, P.; Pearson, M.; McConnell, D. B.; Ciulli, A. BAF Complex Vulnerabilities in Cancer Demonstrated via Structure-Based PROTAC Design. *Nat. Chem. Biol.* **2019**, *15* (7), 672−680.
(40) Dhalluin, C.; Carlson, J. E.; Zeng, L.; He, C.; Aggarwal, A. K.; Zhou, M. M.; Zhou, M. M. Structure and Ligand of a Histone Acetyltransferase Bromodomain. *Nature* **1999**, *399* (6735), 491−496.
(41) Owen, D. J.; Ornaghi, P.; Yang, J. C.; Lowe, N.; Evans, P. R.; Ballario, P.; Neuhaus, D.; Filetici, P.; Travers, A. A. The Structural Basis for the Recognition of Acetylated Histone H4 by the Bromodomain of Histone Acetyltransferase Gcn5p. *EMBO J.* **2000**, *19* (22), 6141−6149.
(42) Flynn, E. M.; Huang, O. W.; Poy, F.; Oppikofer, M.; Bellon, S. F.; Tang, Y.; Cochran, A. G. A Subset of Human Bromodomains Recognizes Butyryllysine and Crotonyllysine Histone Peptide Modifications. *Structure* **2015**, *23* (10), 1801−1814.
(43) Mashtalir, N.; Dao, H. T.; Sankar, A.; Liu, H.; Corin, A. J.; Bagert, J. D.; Ge, E. J.; D'Avino, A. R.; Filipovski, M.; Michel, B. C.; Dann, G. P.; Muir, T. W.; Kadoch, C. Chromatin Landscape Signals Differentially Dictate the Activities of MSWI/SNF Family Complexes. *Science* **2021**, *373* (6552), 306−315.
(44) Ali, M.; Yan, K.; Lalonde, M. E.; Degerny, C.; Rothbart, S. B.; Strahl, B. D.; Côté, J.; Yang, X. J.; Kutateladze, T. G. Tandem PHD Aingers of MORF/MOZ Acetyltransferases Display Selectivity for Acetylated Histone H3 and Are Required for the Association with Chromatin. *J. Mol. Biol.* **2012**, *424* (5), 328−338.
(45) Zeng, L.; Zhang, Q.; Li, S.; Plotnikov, A. N.; Walsh, M. J.; Zhou, M. M. Mechanism and Regulation of Acetylated Histone Binding by the Tandem PHD Finger of DPF3b. *Nature* **2010**, *466* (7303), 258−262.
(46) Chung, C.-W.; Coste, H.; White, J. H.; Mirguet, O.; Wilde, J.; Gosmini, R. L.; Delves, C.; Magny, S. M.; Woodward, R.; Hughes, S. A.; Boursier, Ev.; Flynn, H.; Bouillot, A. M.; Bamborough, P.; Brusq, J.-M. G.; Gellibert, F. J.; Jones, E. J.; Riou, A. M.; Homes, P.; Martin, S. L.; Uings, I. J.; Toum, J.; Clement, C. A.; Boullay, A.-B.; Grimley, R. L.; Blandel, F. M.; Prinjha, R. K.; Lee, K.; Kirilovsky, J.; Nicodeme, E. Discovery and Characterization of Small Molecule Inhibitors of the BET Family Bromodomains. *J. Med. Chem.* **2011**, *54* (11), 3827−3838.
(47) Mujtaba, S.; Zeng, L.; Zhou, M. M. Structure and Acetyl-Lysine Recognition of the Bromodomain. *Oncogene* **2007**, *26*, 5521−5527.